PAPER

The notion of a plastic material spin in atomistic simulations

IOP Publishing Modelling and Simulation in Materials Science and Engineering

Modelling Simul. Mater. Sci. Eng. **24** (2016) 085010 (16pp) doi:10.1088/0965-0393/24/8/085010

The notion of a plastic material spin in atomistic simulations

D Dickel[1], T G Tenev[2], P Gullett[2] and M F Horstemeyer[1,2]

[1] Center for Advanced Vehicular Systems, Mississippi State University Starkville, MS 39759, USA
[2] Bagley College of Engineering, Mississippi State University Starkville, MS 39759, USA

E-mail: doyl@cavs.msstate.edu

Received 7 July 2016, revised 23 September 2016
Accepted for publication 6 October 2016
Published 2 November 2016

Abstract

A kinematic algorithm is proposed to extend existing constructions of strain tensors from atomistic data to decouple elastic and plastic contributions to the strain. Elastic and plastic deformation and ultimately the plastic spin, useful quantities in continuum mechanics and finite element simulations, are computed from the full, discrete deformation gradient and an algorithm for the local elastic deformation gradient. This elastic deformation gradient algorithm identifies a crystal type using bond angle analysis (Ackland and Jones 2006 *Phys. Rev.* B **73** 054104) and further exploits the relationship between bond angles to determine the local deformation from an ideal crystal lattice. Full definitions of plastic deformation follow directly using a multiplicative decomposition of the deformation gradient. The results of molecular dynamics simulations of copper in simple shear and torsion are presented to demonstrate the ability of these new discrete measures to describe plastic material spin in atomistic simulation and to compare them with continuum theory.

Keywords: copper, atomistics, plastic spin, deformation gradient

(Some figures may appear in colour only in the online journal)

1. Introduction

Modern problems in materials science and engineering involve physical phenomena at a number of length scales from the macroscopic down to the atomistic. Because of the necessity that models and theory at disparate length scales agree with each other in order to provide reliable predictions, as well as with experimental evidence, much research has been focused on the development of tools to link atomistic and continuum scales [2].

One of the great challenges in connecting atomistic and continuum scales is the lack of common objective measures of deformation. While the deformation gradient has become the basis of understanding deformation in continuum mechanics, atomistic measures of deformation have only appeared relatively recently. While a number of useful measures now exist on the microscopic scales (including centro-symmetry [3] and slip vectors [4]), these measures are not used at continuum scales, and indeed, it is unclear if analogous measures exist which can be derived from continuum variables. The alternative has been to compute measures on the atomistic scale that are analogous to continuum quantities. A number of methods for computing strain tensors exist in the literature [5–10].

The basis for understanding of strain in continuum mechanics, however, is the deformation gradient. From this tensor and straightforward extensions of it, the majority of continuum deformation variables can be determined. Algorithms to compute a tensor quantity in discrete simulations corresponding to the continuum deformation gradient have been successfully implemented by Horstemeyer and Baskes [8], Gullett *et al* [6], Zimmerman *et al* [9] and Shimizu *et al* [11].

In addition to measures of the assumed elastic deformation, inelastic continuum mechanics has made great gains in understanding the role of plasticity, including dislocation formation and motion, related to a macroscopic perspective of mechanical materials properties. Furthermore, the plastic spin has been shown to be a relevant continuum variable for large deformations of anisotropic materials [12–16]. The plastic spin, commonly defined as the continuum spin relative to the spin of the material, is relevant to large (finite) deformations of anisotropic materials [17]. An example of a large deformation is the forming of metal sheets, such as during the rolling process of materials. Rolling introduces preferred directions in the macroscopic behavior, which gives rise to an anisotropic behavior in plastic deformations. These preferred directions rotate with the evolution of plasticity giving rise to plastic spin [16] sometimes referred to as texture. See [18] for a review of texture and deformation induced anisotropy. The kinematics of the substructure are what define the material symmetries. Such kinematics are not necessarily identical to the kinematics of the continuum, and the plastic spin accounts for the difference between the two. For example, in the case of a single crystal, the substructure symmetries are specified by the crystal lattices director vectors. Under large strains these may have spin $\boldsymbol{\omega}$, also referred to as constitutive spin [19], while at the same time the macroscale continuum may have spin $\mathbf{W}$. According to [14], the difference,

$$\mathbf{W}^p = \mathbf{W} - \boldsymbol{\omega} \tag{1}$$

is the plastic spin. We use boldface to denote vector or tensor quantities and the distinction between the two depends on the context. In this case both $\boldsymbol{\omega}$ and $\mathbf{W}$ are second rank tensors. Although in this example of a single crystal we identified the substructure spin with the spin of the director vectors, the substructure spin concept could be generalized to an arbitrary internal state variable (ISV) that represents some directional anisotropy within the material [19]. The aforementioned formulation of the plastic spin concept is not the only one used in the literature. Another frequent formulation is to identify the plastic spin with the antisymmetric part of the plastic velocity gradient. Although in certain situations the two formulations coincide, in general, they are not equivalent. This appears to have caused some confusion in the literature as discussed by Van der Giessen [20]. Dafalias [19] attempted to rectify the situation by providing a more abstract definition with fewer ad hoc assumptions.

Starting in the 1950s, Nye [21], Bilby *et al* [22], and Kröner [23] proposed, within the context of crystal plasticity, the multiplicative decomposition of the deformation gradient $\mathbf{F}$ into plastic and elastic parts, $\mathbf{F} = \mathbf{F}^e\mathbf{F}^p$. Later, this idea was extended to general continuum plasticity by Lee and Liu [24]. Presently the multiplicative decomposition of the deformation

gradient serves as the starting point for practically any study in plasticity, including the plastic spin. Conceptually, the material first undergoes a plastic deformation via $\mathbf{F}^p$ into a relaxed intermediate configuration that is not necessarily compatible, followed by an elastic deformation via $\mathbf{F}^e$ that restores compatibility. In reality, plastic and elastic deformations occur simultaneously. Nevertheless, the intermediate configuration can be isolated, and therefore defined, as the resulting configuration after removing all stresses from the end configuration. In the context of such intermediate configuration, consider the plastic velocity gradient $\mathbf{L}^p$ derived based on the plastic deformation gradient $\mathbf{F}^p$ as follows,

$$\boldsymbol{L}^p = \dot{\boldsymbol{F}}^p \boldsymbol{F}^{p-1} = \boldsymbol{D}^p + \boldsymbol{W}^p \tag{2}$$

$$\boldsymbol{D}^p \equiv 1/2[\boldsymbol{L}^p + (\boldsymbol{L}^p)^T] \tag{3}$$

$$\boldsymbol{W}^p \equiv 1/2[\boldsymbol{L}^p - (\boldsymbol{L}^p)^T] \tag{4}$$

where $\mathbf{D}^p$ and $\mathbf{W}^p$ are the symmetric and antisymmetric parts of $\mathbf{L}^p$, respectively. The second rank tensor $\mathbf{D}^p$ represents the plastic rate of deformation, while $\mathbf{W}^p$ represents the plastic component of the continuum spin. In much of the literature $\mathbf{W}^p$ is called the plastic spin, which appears to be an overlapping, but not necessarily equivalent definition to the one given earlier according to equation (1). It is this definition (equation (2)) of the plastic spin, also known in the literature as the material plastic spin, to differentiate it from $\mathbf{W}^p$ from equation (1), for which we will find an atomistic approximation. While Tucker *et al* [10] used an atomistic representation of the full deformation gradient to model the total spin, the authors know of no method for approximating the plastic material spin on the atomistic scale. Of central importance in such an approximation (as identified in [10]) is a decoupling of elastic and plastic contributions to the deformation gradient.

In this paper, we develop a set of algorithms for calculating the per-atom elastic deformation gradient for face-centered cubic (fcc), body-centered cubic (bcc), and hexagonal close-packed (hcp) crystal structures, determined using bond angle analysis [1]. This tensor is then used in conjunction with the full deformation gradient, using the method of Gullett *et al* [6], to calculate the plastic deformation gradient on a per-atom basis. Once both components of the deformation gradient have been isolated, the plastic material spin can be derived from the time-varying plastic deformation gradient. Section 2 briefly reviews the theoretical treatment of the continuum level deformation measures and discusses the concept of plastic spin. In section 3, algorithms are detailed for computing the local elastic deformation gradient for every atom in the system. Section 4 demonstrates the reliability of these new measures using atomistic simulations of deformation in copper. Qualitative comparisons are then made to finite element simulations of torsion in copper [25]. Finally, the work presented is summarized and averaging approaches for comparison with continuum calculations are discussed.

2. Continuum mechanics, plasticity, and the plastic spin

In this section, we will briefly summarize the continuum mechanics concept of the deformation gradient and its extension to continuum plasticity theory. Assuming a fixed Cartesian system containing a continuous body with locations in the body described by a position vector, we can define an alteration of that body, χ, which maps the initial position of a part of the body to a new position after the deformation. The set of initial positions will be termed the reference configuration, Ω_0, with position vectors, $\mathbf{X}$ and the new positions, termed the current

configuration, Ω_1 with position vectors, **x**. The reference and current configurations are related through the deformation by:

$$\mathbf{x} = \chi(\mathbf{X}) \tag{5}$$

If the body is continuous, we can define the local deformation at a point as the gradient of the alteration

$$\mathbf{F} \equiv \frac{\partial \mathbf{x}}{\partial \mathbf{X}} \tag{6}$$

in terms of a second order, two-point tensor, **F** as the deformation gradient. For an infinitesimally small vector, dX, it can also be shown from [6] that

$$\mathrm{d}\mathbf{x} = \mathbf{F}\mathrm{d}\mathbf{X} \tag{7}$$

From equation (7) the role of **F** is the mapping a differential vector, $d\mathbf{X}$, at **X** in the reference configuration to d**x**, at **x** in the current configuration.

As mentioned above the deformation gradient is typically multiplicatively decomposed into two components: the elastic deformation gradient, representing reversible deformation (e.g. a deformation that would vanish if the sample were unloaded), and a plastic deformation gradient, representing the irreversible inelastic movement of atoms as the result of dislocation motion or other mechanisms.

Given the deformation gradient or its elastic and plastic parts, one can further specify a time derivative of the deformation gradient assuming a current configuration, and hence, a velocity gradient, as in equation (2). Again, we will consider below the anti-symmetric part of the plastic velocity gradient as the plastic material spin.

3. Elastic deformation gradient algorithm

At the atomistic scale, the elastic deformation gradient should describe the change in the lattice vectors for a given crystal structure from their initial values. If the lattice vectors of a unit cell are compared between the reference and current configurations, this will provide the same information as the continuum elastic deformation gradient, namely the elastic distortion of the lattice. We propose defining the elastic deformation gradient for a given atom in an atomistic simulation as the proportional change in orthogonal lattice vectors from the reference to the current configuration:

$$\mathbf{F}^e = \frac{\Delta \mathbf{x}}{\Delta \mathbf{X}} \tag{8}$$

where $\Delta\mathbf{x}$ is a lattice vector in the current configuration and $\Delta\mathbf{X}$ is one in the reference configuration. In the case where the axes of the reference configuration are aligned with the orthogonal lattice vectors of crystal lattice, the components of the elastic deformation gradient, F^e_{ij} are given by:

$$F^e_{ij} = \frac{\Delta x_{ij}}{\Delta X_j} \tag{9}$$

where Δx_{ij} is the ith component of lattice vector j in the current configuration and ΔX_j is the length of lattice vector j in the reference configuration. Assuming the three vectors ΔX lie along the coordinate axes, equation (9) will give the elastic deformation gradient directly. Otherwise, as long as the ΔX are orthogonal, these components can be transformed into a

coordinate system rotated arbitrarily with respect to the crystal lattice by summing the projections of the components of equation (9) onto each of the axes as in the following,

$$F_{ij}^{e} = \sum_{k=1}^{3} \frac{\Delta x_{ik} \Delta X_{jk}}{\Delta X_{1k}^2 + \Delta X_{2k}^2 + \Delta X_{3k}^2} \tag{10}$$

where ΔX_{ij} is now the ith component of reference configuration lattice vector j. Here, the denominator is the square of the length of $\Delta \mathbf{X}_j$. Note that this definition will only work for orthogonal reference vectors ΔX and produces a distinct value of the deformation gradient for every unit cell, which means, in principle, $\mathbf{F}$ will be defined individually for every atom. The challenge that remains is accurately identifying the lattice constants for a given atom. While extension to non orthogonal ΔX is possible by defining a coordinate transformation between the system defined by these vectors and Cartesian coordinates, this has not been attempted here as orthogonal axes can be easily defined for typical metal crystal structures.

In order to do this, one must first identify the crystal structure of the atom in question. We have chosen to accomplish this using bond-angle analysis (BAA) [1]. This method was chosen both because of its effectiveness in identifying crystal structures common in metals as well as its commonality with our method, presented below, of determining lattice vectors using bond angles. If BAA indicates that an atom is in a given crystal structure, we can proceed knowing that certain bond angles will necessarily exist for the target atom. By probing the atoms which comprise these pairs, we can identify the three independent lattice vectors. Because of their unique character with regard to the bond angles present, individual algorithms must be developed for every crystal structure. Below we present our algorithms for BCC, FCC, and HCP crystals.

3.1. Body-centered cubic

We define the lattice vectors of a BCC cell based on the location of second nearest neighbors. The bond angle between two distinct second nearest neighbors in an ideal cell will be either 90 or 180 degrees. In the deformed cell, bond angle analysis will recognize these angles if they are between 78.8 and 101.2 degrees (90 degree ideal bond angle) or above 160.9 degrees (180 degrees). Sufficient deformation to either no longer consider a pair outside of this range or to include a bond angle between nearest neighbors will cause BAA to no longer recognize the cell as BCC, so the success of the BAA algorithm ensures the success in determining the lattice vectors. Second nearest neighbors are identified by the presence of 90 degree bond angles associated with that atom. Once all 6 s nearest neighbors have been identified, pairs can be constructed based on atoms with a 180 degree bond angle. The vector between each of these pairs is then defined as twice a lattice vector, $\mathbf{X}_i$ (see figure 1). It is possible for BAA to recognize a crystal as BCC even if not all of the second nearest neighbors are found. If this happens, it will still be the case that 90 degree angles will only occur between second nearest neighbors, and each of the 3 primitive axes will always contain at least 1 s nearest neighbor. In the event that one of the pair used to define a lattice vector is missing, the lattice vector is instead defined as the vector for the atom under consideration to the second nearest neighbor that is found on that axis.

3.2. Face-centered cubic

Primitive vectors for atoms identified as face-centered cubic by BAA are chosen by first finding the primitive vectors in the dual space. The twelve nearest neighbors of a face centered

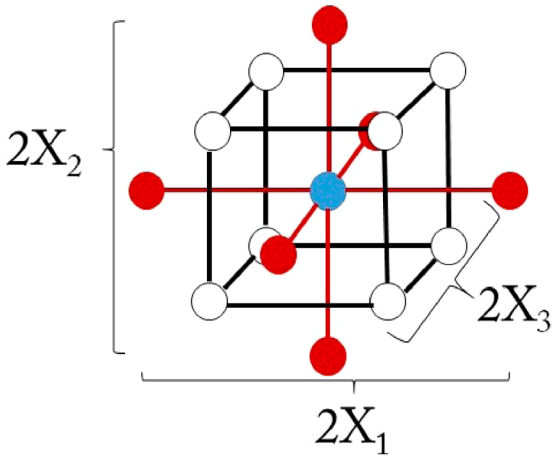

Figure 1. Undeformed body-centered cubic structure. The solid colored atoms (red online) are the second nearest neighbors of the atom for which the deformation is being considered, identified by the 90 degree angle between them and used to define the lattice vectors.

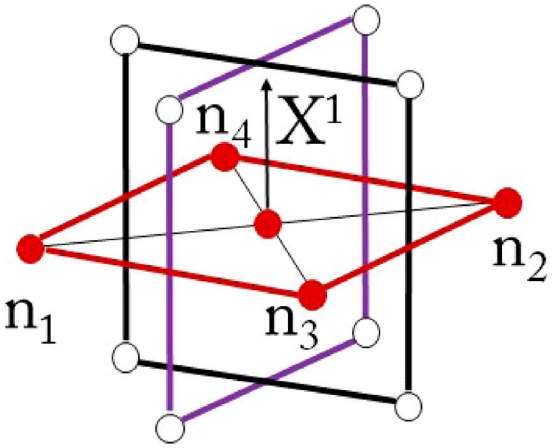

Figure 2. Undeformed face-centered cubic structure. The three planes used to determine the dual space vectors are outlined. The solid colored atoms are one set of coplanar atoms (denoted n_1 through n_4), from which a dual space vector can be determined. The vector X^1 is found from the cross product of the vector connecting atom n_1 and n_2 and the vector connecting n_3 and n_4. Once all three dual space vectors, X^i have been found, the lattice vectors, X_i can be determined using equation (12).

cubic atom can be grouped into three groups of four coplanar atoms with 90 degree angles between adjacent members (see figure 2). As in the BCC case, atoms can be grouped based on the presence of 90 and 180 degree angles which BAA will only find among the set of four atoms in each {1 0 0} plane. Once the nearest neighbors have been grouped into their coplanar sets, dual space primitive vectors are defined by the cross product of the two vectors between neighbors with a 180 degree angle. The magnitude of these vectors will each equal the area of the side of the unit cell to which the coplanar atoms belong.

$$\mathbf{X}^i = \mathbf{N}_{2-1} \times \mathbf{N}_{4-3} \tag{11}$$

where X^i is the dual vector orthogonal to the particular plane, and the vectors, N connect coplanar atoms on opposite sides of the atom for which the vectors are being found (figure 2). The dual vectors can be transformed into the lattice vectors of the unit cell using the relation

$$\mathbf{X}_1 = \frac{\mathbf{X}^2 \times \mathbf{X}^3}{\mathbf{X}^1 \cdot (\mathbf{X}^2 \times \mathbf{X}^3)} \tag{12}$$

with cyclic permutations giving the relation for $\mathbf{X}_2$ and $\mathbf{X}_3$ as well. Note here that $\mathbf{X}^1 \cdot (\mathbf{X}^2 \times \mathbf{X}^3)$ is the volume of the cell centered on the atom in question.

3.3. Hexagonally close packed

Bond angles of 180 degrees will only occur among atoms in the basal plane. In this way, the 6 nearest neighbors in the basal plane can be identified. Similarly neighbors in the plane above and the plane below the target atom can be distinguished by the presence of bond angles with $\cos(\theta) = -\frac{5}{6}$. In the basal plane, we utilize the 3 vectors connecting neighbor pairs with a 180 degree bond angle. One half of each of these vectors is a lattice vector in the basal plane, A_i (each of the three equivalent vectors, $\langle 1\,0\,0\,0 \rangle$, using Bravais–Miller notation). For the out-of-plane vector, the 6 vectors connecting the lower plane atoms to upper plane atoms not directly above them (identified by the unique angle identified above) are averaged to give $\vec{C}$. As was the case with BCC crystals, if not all twelve nearest neighbors are identified, lattice vectors for unpaired neighbors are defined between the atom in question and the unpaired neighbor.

Since the unit vectors in an HCP cell are not all equivalent as was the case with FCC and BCC, and since equation (10) assumes the reference primitive vectors are orthogonal, care must be taken to ensure that consistent directions are found for both the reference and current configuration. The ambiguity in choosing vectors will be discussed below for all three cases. For purposes of calculating the elastic deformation gradient in an HCP cell, we transform from our set of three vectors in the basal plane to vectors which will be orthogonal in an ideal crystal to simplify the analysis and to define it consistently for all three crystal types. To this end, the three in plane lattice vectors are reduced to two orthogonal vectors by selecting half of one of the vectors as X_1, averaging the other two to define X_2. The vector $\vec{C}$, previously defined, is already orthogonal to X_1 and X_2 (see figure 3).

3.4. Algorithm

Once orthogonal primitive vectors are defined for both the reference and current configuration for any of BCC, FCC, or HCP crystals, the elastic deformation gradient can be computed from equation (10). However, since for BCC and FCC (and in plane for HCP), the vectors are all equivalent and thus can be arbitrarily mixed, the vectors in the current configuration must be mapped and oriented one-to-one with vectors in the reference configuration. This is done using the assumption that the elastic deformation is small and hence, a unit vector in the current configuration will correspond to the reference configuration vector with which it is most parallel (smallest angle between them). In the case of pure (non-rotational) strains this will always be the case for structures which can be correctly identified by bond-angle analysis. In the case of rotations greater than $\sim$45 degrees, the algorithm will not correctly match primitive directions between the reference and current configurations, since current configuration vectors will be matched to the reference configuration vector they align most closely with. However, by considering the deformation gradient for some large time t between reference

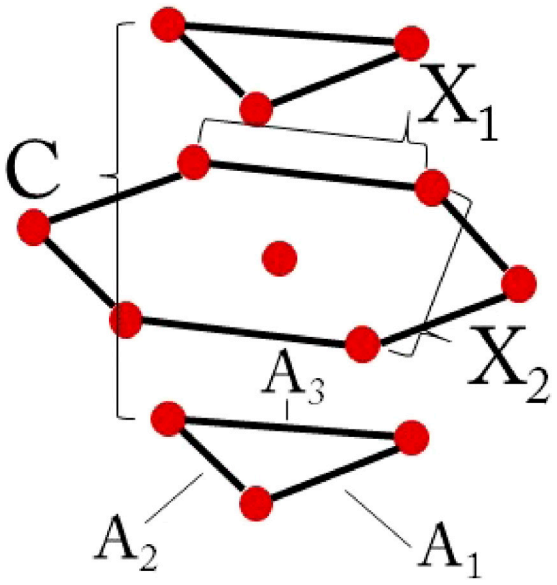

Figure 3. Undeformed hexagonally close packed structure. The vector, $\vec{c}$ is determined from the average vector connecting the planes above and below the basil plane of the atom in question. The interchangeable lattice vectors A_i are found using opposite pairs of atoms in the Basil plane. These 3 vectors can be reduced to the two orthogonal vectors X_1 and X_2 for the calculation of the deformation gradient.

and current configurations as the product of a number of smaller deformations (see [6]) each occurring over time Δt, where the rotation between configurations is small, the correct elastic deformation gradient can be computed since every individual deformation gradient will correctly match current unit vectors to the reference configuration.

Table 1 summarizes the algorithm for calculating the elastic and plastic deformation gradients. After the elastic deformation gradient is determined, the full deformation gradient is found following the method of Gullett *et al* [6]. We note that other methods exist for computing the deformation gradient (including that of Falk [26] and of Mott *et al* [7]). While, in principle, the decomposition using the elastic deformation gradient should work with any definition of the full deformation gradient, most suffer from limitations as described in [6] including difficulty in either computational expense or the appearance of fictious strains in accurately describing systems with large plastic flow or rigid body rotations. For this reason, and because it also calculates the deformation gradient on a per-atom basis, [6] has been used to complete the decomposition. A brief description of this method follows.

The deformation of an atom m is described by the relative motion of its neighbors. If atom n is located at position $\mathbf{X}^n$ in the reference configuration and $\mathbf{x}^n$ in the current configuration, there exists a mapping between the displacements in the reference and current configurations, $\Delta\mathbf{X}^{mn}$ and $\Delta\mathbf{x}^{mn}$:

$$\Delta\mathbf{x}^{mn} = \mathbf{F}^m \cdot \Delta\mathbf{X}^{mn} \tag{13}$$

where $\mathbf{F}^m$ is the deformation gradient at atom m. $\mathbf{F}^m$ is then selected to minimize the l^2 norm, ϕ^m, of the difference between $\Delta\mathbf{x}^{mn}$ and $\mathbf{F}^m \cdot \Delta\mathbf{X}^{mn}$. This is accomplished with the following definition of the deformation gradient

$$\mathbf{F} = \mathbf{A}\mathbf{D}^{-1} \tag{14}$$

Table 1. The algorithm for the computation of the plastic deformation gradient for each individual atom.

Deformation gradient decomposition
1: Determine crystal structure of atom in reference and current configuration using bond angle analysis [1]
2: Find lattice vectors in reference and current configuration (section 3.1–3.3)
3: Match lattice vectors between reference and current configuration
4: Compute $\mathbf{F}^e$ (equation (10))
5: Compute $\mathbf{F}$ [6]
6: Compute $\mathbf{F}^p$ from: $\mathbf{F}^p = \mathbf{F}^{e-1}\mathbf{F}$

where $\mathbf{D}$ and $\mathbf{A}$ are the 3×3 matrices

$$\mathbf{D} = \sum_n \Delta\mathbf{X}^{mn}\mathbf{X}^{mnT} w_n$$
$$\mathbf{A} = \sum_n \Delta\mathbf{x}^{mn}\mathbf{X}^{mnT} w_n \tag{15}$$

and w_n is a weighting function based on the distance to a given neighbor.

Given the elastic and total deformation gradients, the plastic deformation can then be found directly by solving the multiplicative decomposition of the deformation gradient for F^p:

$$\mathbf{F}^p = \mathbf{F}^{e-1}\mathbf{F} \tag{16}$$

Given these quantities, extension to other continuum mechanics quantities is straightforward. Time derivatives are performed using a finite difference scheme between time steps. However, as will be discussed below, time averaging is necessary to derive coherent results for the plastic spin. We also note here that, as with the deformation gradient derived by Gullett *et al* [6], the quantities derived here are not defined as a general function of position in space. Rather, the deformation gradient as well as its elastic and plastic parts defined only for each atom at its atomic position. As such, spatial averaging would be necessary for direct comparison with continuum results.

4. Application to molecular dynamics simulations

We begin by demonstrating the ability of the algorithms of section 3 to accurately determine the elastic deformation gradient for small strains away from equilibrium. All of the simulations shown were performed in LAMMPS [27]. Figure 4 shows small FCC, BCC, and HCP crystal cells of copper under a small shear strain. With the top and bottom row of atoms held fixed, the system is heated to 300 K using a Nosé–Hoover thermostat. Then, a constant velocity is applied to the top row of atoms and the crystal is allowed to deform under this constant strain rate. The system is periodic in the z-direction (into the page) and fixed boundaries are used along the x-axis. Atoms along the boundary in the y direction are left free. While copper is only metastable under this potential in BCC and HCP arrangements and may not accurately describe the evolution of the system, the particular potential is irrelevant for the example given here, as long as no plastic deformation is observed. We merely demonstrate that the elastic deformation gradient for each crystal structure is consistent (up to some thermal noise) with the externally applied strain. We now discuss the algorithm presented in table 1 for the particular examples given in figure 4.

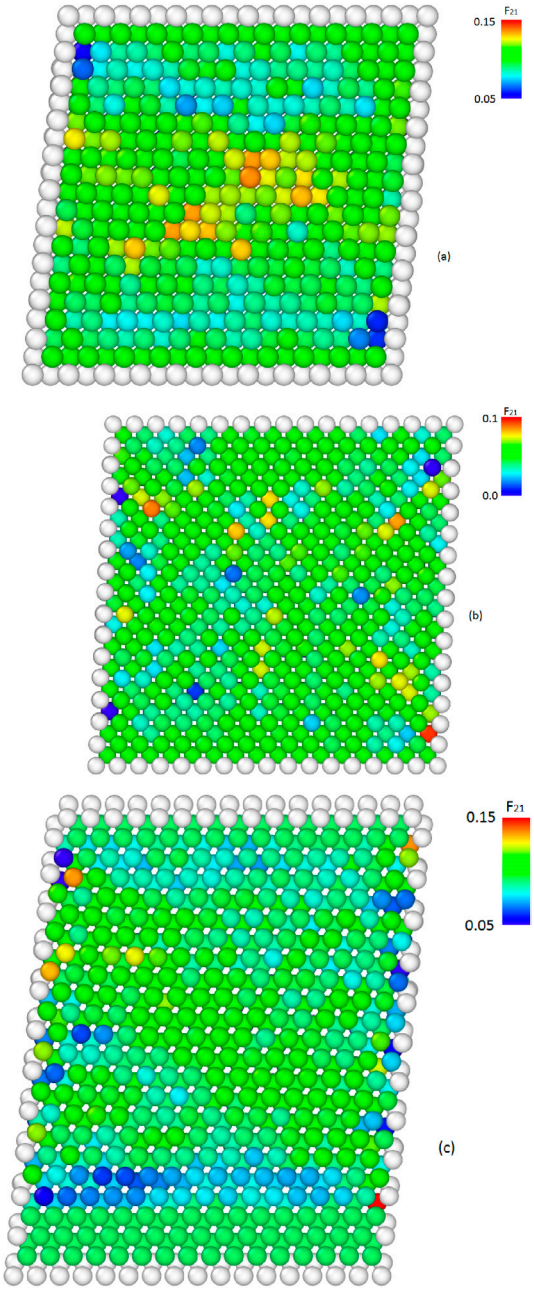

Figure 4. Simply sheared FCC (a), BCC (b), and HCP (c) single crystals at a strain of 5% (2.5% for BCC). The simulation was run at a temperature of 300 K with a strain rate of 10^{10} s^{-1}. All components of the elastic deformation gradient computed using the algorithm in table 1 are approximately zero for off diagonal component and one for diagonal components, except F_{21} which is approximately 0.1 (0.05 for BCC) as should be expected, corresponding to a strain of 0.05 (0.025). Atoms are colored by the measured value of F^e_{21}. The plastic deformation gradient is computed to be approximately the identity matrix as there is no plastic deformation present.

For every atom in the simulation, the crystal structure in the reference (undeformed) and current state is computed. Atoms along the boundaries are left undetermined because a crystal structure cannot be determined for them by BAA (hence they are left white in the figures). Then, using the methods of section 3 for the particular crystal structure, the lattice vectors for each atom are determined in both the reference and current configuration. Next, for each atom, these vectors are matched between the two configurations. In this case, where the net rotation is small, this is straight forward. However, if large enough shear strains were applied such that vectors might be mixed between reference and current configuration, intermediate time steps could be employed as the lattice vectors should change smoothly over time (see section 3.4). Finally, the deformation gradients (elastic and total) for each individual atom can be calculated using equation (10) and Gullett *et al* respectively. The plastic deformation gradient is then directly computed, on a per-atom basis, from these. This gives the correct elastic and plastic deformation gradient up to the point where BAA can no longer identify the crystal structure. In a real material, plastic deformation would normally become a factor before BAA will uniformly fail. To demonstrate the effectiveness of this method in decoupling elastic and plastic strain, we deform an FCC lattice of copper atoms under simple shear past the point of dislocation formation. The atoms are heated to 300 K with the bottom and top row of atoms fixed with some initial velocity. The motion of the atoms in the bulk is covered by a modified embedded atom method (MEAM) potential for copper [28]. The lattice is oriented for double slip under the exerted strain. Figure 5 shows elastic and plastic deformation gradients at a strain of 20% for an entire crystal. It also shows the evolution of the relevant part of the elastic and plastic deformation gradient tensor for two different atoms. The first atom is not directly involved in any plastic deformation gradient (atom 841). As such, its plastic deformation gradient remains close to zero (this is due to a slight mismatch between the methods for calculating the full deformation gradient and the elastic deformation gradient. As can be seen in figure 5(d), this mismatch is small compared to the deformation caused by a single dislocation.) Atom 2161 has two distinct dislocations pass through it over the course of the simulation, creating the 2 jumps in $\mathbf{F}^p_{21}$. Both atoms show a gradual increase in elastic deformation which drops as dislocations are formed to relieve the resulting stress. It should be noted here that for atoms whose crystal structure has changed, we do not have a method to define an elastic deformation gradient and, for purposes of these examples, assume that it is the identity tensor. This means that if the crystal structure has changed from the reference configuration, all of the strain is considered plastic. It may be possible to relate primitive vectors between different crystal structures (for example using the Bain transformation between FCC and BCC crystals or close packed plane vectors in FCC to compare with HCP). The possibilities of defining elastic strain between different crystal structures has not been considered here, however. The effect of dislocation motion can be seen in figure 5, where the onset of plasticity greatly reduces the elastic strain. We can also see the local effect of dislocation motion, reducing elastic strain in regions with increased plastic strain. The paths traced by dislocations can also be seen in the crossed lines of increased plastic deformation. Because the elastic (and hence the plastic) deformation gradient is only defined using the local atom neighbors, plastic deformation will only appear in atoms through which the core of the dislocation has passed. Figure 6 shows the effects of a loading and unloading cycle, showing the presence of plastic deformation even in a sample which is macroscopically unstrained. The system was sheared as above up to a strain of 25%. The net motion was then reversed and the top row of atoms returned to its initial position. As expected, plastic deformation remains in the unloaded configuration, while the elastic deformation gradient (not shown) is close to zero for every atom. This can be directly compared with internal state variable models where the history of the material must be considered in determining its mechanical properties.

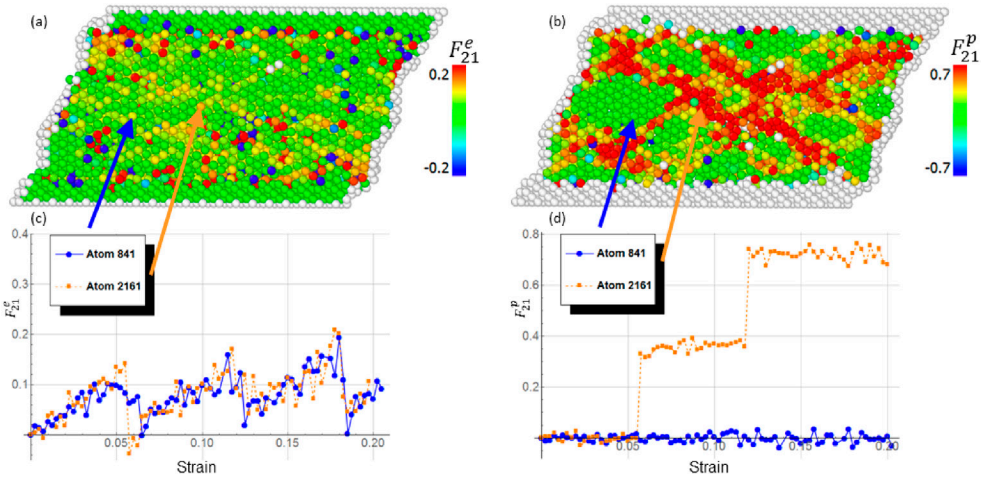

Figure 5. A slab of copper atoms sheared to 20% strain. The F^e_{21} component of the elastic deformation gradient (a) is approximately uniform and increased strain is randomly distributed. The F^p_{21} component of the plastic deformation gradient (b) is considerably higher and concentrated in the path traced by dislocations that have moved through the sample (along $\langle 1\,1\,0\rangle$ directions). Figures 5(c) and (d) show F^e_{21} (c) and F^p_{21} (d) as a function of applied strain for 2 different atoms. The atom designated 841 does not experience any plastic slip. Atom 2161 has dislocations move through it at two different times, indicated by the two steps in F^p_{21}. Note: Because BAA is unable to determine the crystal structure of boundary atoms, the components of the deformation gradient cannot be found. In addition, the fixed atoms at the top and bottom also cannot be resolved by BAA above a certain strain, leading to a failure of the algorithm for $\mathbf{F}^p$. These atoms are colored in white.

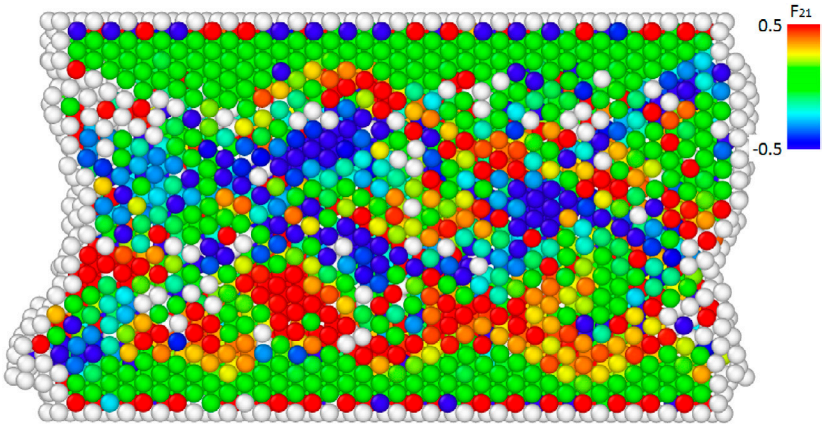

Figure 6. The F^p_{21} component of the plastic deformation gradient of a single crystal slab of copper, deformed to 25% shear strain and returned to zero net strain. The evidence of dislocation motion (and on a continuum scale, work hardening) can be clearly seen by the increased magnitude of the plastic deformation gradient.

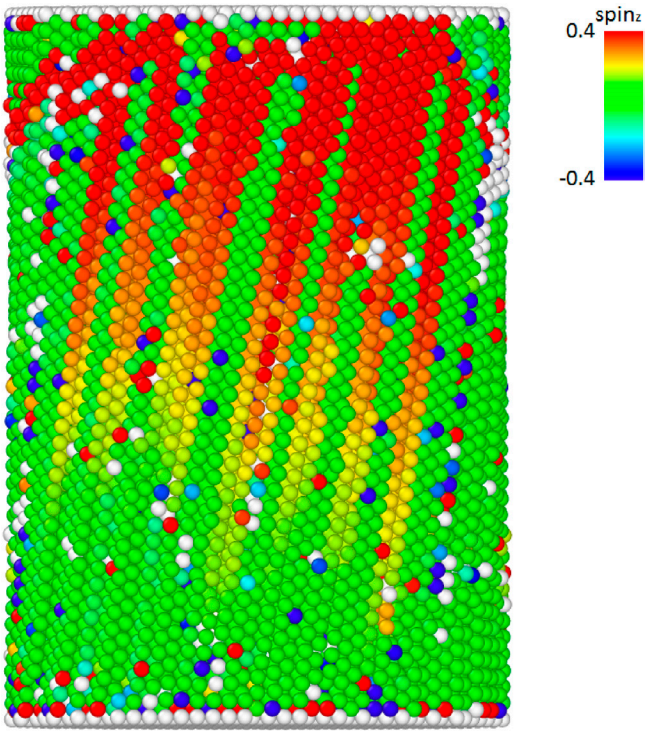

Figure 7. A copper micropillar under simple torsion up to 30°. The plastic material spin can be observed by the color differentiation. Color indicates the plastic material spin in the z (vertical) direction. Spin is localized along the paths of dislocations as would be expected. It can also be observed that plastic material spin is not evenly distributed around the cylinder, but rather concentrated on opposite sides.

Finally, having verified that the time independent strain quantities accurately reflect what would be expected from continuum mechanics, we can consider the more complicated case of plastic spin. However, we must first consider what the time derivative (equation (2)) will mean for our algorithm.

Tucker *et al* [10] highlights different methods for calculating the velocity gradient. The first two of these methods involve using the instantaneous velocities of the particles directly, while the third uses the difference in $\mathbf{F}$ between time steps. In the case of a dislocation moving through a crystal (see for example: figure 5(b)), it is clear that the plastic deformation increases in discrete units (proportional to the Burgers vector) and so the plastic velocity gradient is only nonzero in the instant the core of the dislocation passes through the atom in question. Clearly, to compare to a meaningful continuum level quantity, instantaneous measures of the velocity gradient will no be useful and averaging should be done both spatially and temporally. To this end, the derivatives in equation (2) are computed using a simple backward difference method between consecutive times steps. Averaging can then, in principle, be taken over all the atoms in a given region to find a plastic spin over a region comparable to continuum results. Figure 7 shows this method as applied to the torsion of a copper pillar. The presence of spin can be seen around the path of dislocations in the pillar.

5. Conclusion

A new method for calculating the plastic material spin from discrete atomic data, using the total deformation gradient and a new algorithm for finding the elastic deformation gradient is presented. By decoupling the elastic and plastic contributions to deformation in atomistic simulation, additional quantities, such as the plastic material spin, can be compared between discrete and continuum length scales. The proposed calculation of the elastic deformation gradient follows bond-angle analysis, using the bond angles present in a given crystal structure to define lattice vectors which can be compared between reference and current configurations.

The plastic deformation gradient, computed in this manner, will reflect the motion of dislocations or other plastic defects through a given atom at some time in its history. The motion of a dislocation through an atom will appear as a jump in $\mathbf{F}^p$. By time averaging over this discontinuous jump, a plastic velocity gradient and, from there, a plastic spin, can be calculated. We reiterate here that the derived quantities, including elastic and plastic deformation gradients, and the plastic spin, are defined on a per-atom basis. In order for a meaningful comparison to be made between these values and a continuum quantity, spatial averaging must be performed. The two most direct methods are as follows: first, assuming a suitable length scale separation between the macroscopic and the microscopic, a given volume of atoms could be made tantamount to a macroscopic continuum point, with the continuum variable being related to the simple average of the values within that volume element. As a second, and more robust option, the Irving–Kirkwood method [29–32] use a localization function to define a spatial support over which the average is computed. Such a localization could take the form

$$\tilde{\omega}(\mathbf{X}) = \sum_n \omega_n \phi(\mathbf{X} - \mathbf{X}_i) \tag{17}$$

Here, ϕ would be a weight function and $\tilde{\omega}$ would be the spatially resolved plastic spin. A complete description of an atomistically derived plastic spin requires the use of such a kernel function and will be the subject of future work.

Since the formulation utilizes position vectors and neighbor lists, considering only nearest neighbors (and second nearest neighbors for BCC crystals), the computational complexity, excluding the generation of neighbor lists scales linearly with the number of atoms. Once both the total deformation gradient and the elastic gradient are constructed, all other local quantities from continuum plasticity theory can be computed directly.

Simple shearing of a copper slab showed the accuracy of the algorithm in decoupling elastic and plastic deformation. The motion of dislocations increased the plastic deformation in their wake and relaxed the elastic deformation throughout the crystal. The simple torsion of a nanopillar of copper atoms was simulated to evaluate the computed plastic spin. The results demonstrate the ability of this method to determine both the elastic and plastic contributions to deformation in a regular crystalline metal.

Use of this method will help to strengthen the information bridge between discrete atomic simulation and continuum simulations on the smallest length scales. By introducing the continuum metrics into the atomistic scale, the ability to validate accurate continuum models, as well as a deeper understanding of the discrete mechanisms which facilitate meso- and macroscopic behavior will be greatly enhanced.

Acknowledgments

The authors would like to thank the Center for Advanced Vehicular Systems (CAVS) at Mississippi State University and the U.S. Army Engineer Research and Development

Center (ERDC) for supporting this work. Effort sponsored by the Engineering Research & Development Center under Cooperative Agreement number W912HZ-15-2-0004. The views and conclusions contained herein are those of the authors and should not be interpreted as necessarily representing the official policies or endorsements, either expressed or implied, of the Engineering Research & Development Center or the U.S. Government.

References

[1] Ackland G J and Jones A P 2006 Applications of local crystal structure measures in experiment and simulation *Phys. Rev.* B **73** 054104
[2] Horstemeyer M F 2012 *Integrated Computational Materials Engineering for Metals: Using Multiscale Modeling to Invigorate Engineering Design with Science* (Hoboken: Wiley)
[3] Kelchner C L, Plimpton S J and Hamilton J C 1998 Dislocation nucleation and defect structure during surface indentation *Phys. Rev.* B **58** 11085
[4] Zimmerman J A, Kelchner C L, Klein P A, Hamilton J C and Foiles S M 2001 Surface step effects on nanoindentation *Phys. Rev.* B **87** 165507
[5] Ward D K, Curtin W A and Qi Y 2006 Mechanical behavior of aluminum-silicon nanocomposites: a molecular dynamics study *Acta Mater.* **54** 4441–51
[6] Gullett P M, Horstemeyer M F, Baskes M I and Fang H 2008 A deformation gradient tensor and strain tensors for atomistic simulations *Modelling Simul. Mater. Sci. Eng.* **16** 015001
[7] Mott P H, Argon A S and Suter U W 1992 The atomic strain tensor *J. Comput. Phys.* **101** 140–50
[8] Horstemeyer M F and Baskes M I 1999 Strain tensors at the atomic scale *MRS Proc.* **578** 15
[9] Zimmerman J A, Bammann D J and Gao H 2009 Deformation gradients for continuum mechanical analysis of atomistic simulations *Int. J. Solids Struct.* **46** 238–53
[10] Tucker G J, Zimmerman J A and McDowell D L 2009 Shear deformation kinematics of bicrystalline grain boundaries in atomistic simulations *Modelling Simul. Mater. Sci. Eng.* **18** 015002
[11] Shimizu F, Ogata S and Li J 2007 Theory of shear banding in metallic glasses and molecular dynamics calculations *Mater. Trans.* **48** 2923–7
[12] Dafalias Y F 1983 Corotational rates for kinematic hardening at large plastic deformations *J. Appl. Mech.* **50** 561
[13] Dafalias Y F 1984 The plastic spin concept and a simple illustration of its role in finite plastic transformations *Mech. Mater.* **3** 223–33
[14] Dafalias Y F 1985 The plastic spin *J. Appl. Mech.* **52** 865
[15] Loret B 1983 On the effects of plastic rotation in the finite deformation of anisotropic elastoplastic materials *Mech. Mater.* **2** 287–304
[16] Ulz M H 2011 A finite isoclinic elasto-plasticity model with orthotropic yield function and notion of plastic spin *Comput. Methods Appl. Mech. Eng.* **200** 1822–32
[17] Kratochvil J 1973 On a finite strain theory of elastic-inelastic materials *Acta Mech.* **16** 127–42
[18] Wenk H R and Van Houtte P 2004 Texture and anisotropy *Rep. Prog. Phys.* **67** 1367
[19] Dafalias Y F 1998 Plastic spin: necessity or redundancy? *Int. J. Plast.* **14** 909–31
[20] Van der Giessen E 1991 Micromechanical and thermodynamic aspects of the plastic spin *Int. J. Plast.* **7** 365–86
[21] Nye J F 1953 Some geometrical relations in dislocated crystals *Acta Metall.* **1** 153–62
[22] Bilby B A, Bullough R and Smith E 1955 Continuous distributions of dislocations: a new application of the methods of non-riemannian geometry *Proc. R. Soc.* A **231** 263–73
[23] Kröner E 1960 Allgemeine kontinuumstheorie der versetzungen und eigenspannungen *Arch. Ration. Mech. Anal.* **4** 273–334
[24] Lee E H and Liu D T 1967 Finite strain elastic-plastic theory with application to plane-wave analysis *J. Appl. Phys.* **38** 19–27
[25] Horstemeyer M F, Lim J, Lu W Y, Mosher D A, Baskes M I, Prantil V C and Plimpton S J 2002 Torsion/simple shear of single crystal copper *J. Eng. Mater. Technol.* **124** 322–8
[26] Falk M L 1999 Molecular-dynamics study of ductile and brittle fracture in model noncrystalline solids *Phys. Rev.* B **60** 7062
[27] Plimpton S J 1995 Fast parallel algorithms for short-range molecular dynamics *J. Comput. Phys.* **117** 1–19

[28] Jelinek B, Groh S, Horstemeyer M F, Houze J, Kim S G, Wagner G J, Moitra A and Baskes M I 2012 Modified embedded atom method potential for Al, Si, Mg, Cu and Fe alloys *Phys. Rev.* B **85** 245102
[29] Irving J H and Kirkwood J G 1950 The statistical mechanical theory of transport processes. IV. The equations of hydrodynamics *J. Chem. Phys.* **18** 817–29
[30] Noll W 1955 Die herleitung der grundgleichungen der thermomechanik der kontinua aus der statistischen mechanik *Indiana Univ. Math. J.* **4** 627–46
[31] Hardy R J 1982 Formulas for determining local properties in moleculardynamics simulations: shock waves *J. Chem. Phys.* **76** 622–8
[32] Murdock A I 1983 The motivation of continuum concepts and relations from discrete considerations *Q. J. Mech. Appl. Math.* **36** 163–87